Contents lists available at ScienceDirect

JCIS Open

On the interaction and nanoplasmonics of gold nanoparticles and lipoproteins

Andrea Zendrini [a,b,*], Jacopo Cardellini [b,c], Roberto Frigerio [a,d], Marianna Bertoni [a], Debora Berti [b,c], Paolo Bergese [a,b,e,**]

[a] Department of Molecular and Translational Medicine, Università degli Studi di Brescia, Viale Europa 11, 25123, Brescia, Italy
[b] Center for Colloid and Surface Science (CSGI), Via della Lastruccia 3, 50019, Sesto Fiorentino, Firenze, Italy
[c] Department of Chemistry "Ugo Schiff", Università degli Studi di Firenze, Via della Lastruccia 3, 50019, Sesto Fiorentino, Firenze, Italy
[d] Istituto di Scienze e Tecnologie Chimiche "Giulio Natta"—National Research Council of Italy (SCITEC-CNR), 20131, Milano, Italy
[e] National Inter-university Consortium of Materials Science and Technology (INSTM), Via Giuseppe Giusti 9, 50121, Firenze, Italy

ARTICLE INFO

ABSTRACT

The extracellular space is nanostructured, populated by heterogeneous classes of nanoparticles, e.g., extracellular vesicles and lipoproteins, which "made by cells for cells" mediate intercellular, inter-organ, cross-species, and cross-kingdom communication. However, while techniques to study ENP biology in-vitro and in-vivo are becoming available, knowledge of their colloidal and interfacial properties is poor, although much needed. This paper experimentally shows, for the first time, that the aggregation of citrate-capped gold nanoparticles (AuNPs) triggered by lipid vesicle membranes and the related characteristic redshift of the plasmonic signature also applies/extends to lipoproteins. Such interaction leads to the formation of AuNP-lipoprotein hybrid nanostructures and is sensitive to lipoprotein classes and AuNP/lipoprotein molar ratio, paving the way to further synthetic and analytical developments.

1. Introduction

Up to a few years ago, cell communication was thought to be exclusively regulated through cellular junctions or via the cellular "secretome". This term, coined at the dawn of the 21st century [1], identifies different classes of soluble, active biomolecules (cytokines, hormones, growth factors, etc.) released by cells into the extracellular space and able to modify cell metabolism and activity.

However, the extracellular space also harbors a large variety of secreted endogenous extracellular nanoparticles, making it full-fledged nanostructured. "Made by cells for cells", these biogenic nanoparticles represent an asset of all biological fluids and fully take part in the regulation of physio- and pathological processes of living organisms, including cancer metastasis [2,3], microbiota homeostasis [4], viral infection and immunomodulation [3,5], thus complementing and synergizing with their soluble counterparts.

Extracellular nanoparticles - whose function is shaped by both their molecular and colloidal identity [6] - include, but are not limited to, macromolecular transport complexes [7,8], a variety of lipid membrane-bound vesicles [9] often referred to as extracellular vesicles (Fig. 1, left) [2,10,11], and other lipid nanosized particles called lipoproteins. Lipoproteins cover the transport of lipids across the bloodstream between cells and tissues where lipids are synthesized, processed, and/or stored (lipid metabolism) [12–14]. All lipoproteins are micelle-like nanoparticles with a hydrophobic core made of non-polar lipids (triacylglycerols and cholesteryl esters) surrounded by a monolayer of phospholipids embedding lipid-binding proteins called apolipoproteins (Fig. 1, right). Five main classes of lipoproteins exist - chylomicrons, Very Low-Density Lipoproteins (VLDLs), Intermediate Density Lipoproteins (IDLs), Low-Density Lipoproteins (LDL), and High-Density Lipoproteins (HDL) - which share the common lipoprotein structure given in Fig. 1 but differ for function, size, density, and relative composition.

Besides their long-established use as molecular biomarkers for metabolic and cardiovascular diseases [15–17], natural and engineered lipoproteins proved their potential in the field of nanomedicine, as drug delivery vectors [18–20], adjuvant carriers for vaccines [21,22] and tissue regeneration agents [23].
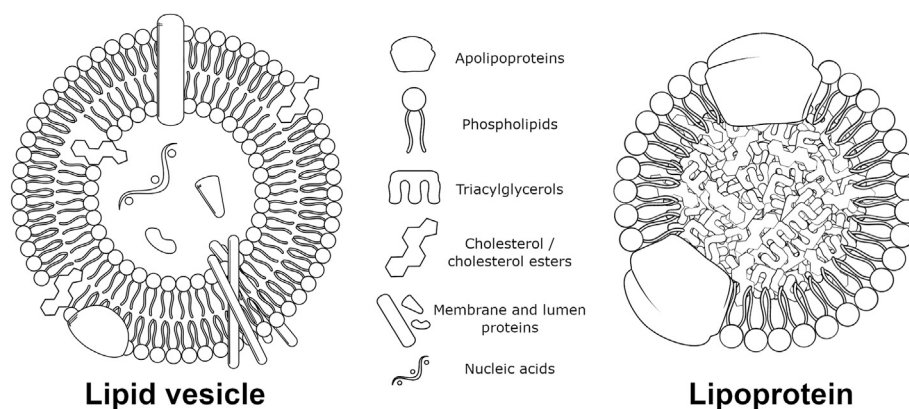
Fig. 1. A sketch of the structure and main components of lipid vesicles and lipoproteins.

The role of a corona made of the protein components of lipoproteins (e.g. apolipoproteins) in enhancing the cellular uptake [24–27] and targeting ability [27–30] of synthetic nanoparticles (NPs) has been investigated. However, the reports on the interaction of lipoprotein NPs with synthetic nanomaterials are scarce. Pioneering works provide evidences on such interaction (in particular using HDLs), describing the formation of a corona of intact or disintegrated lipoproteins on the surface of various types of NPs, including copolymeric [31] and silica particles [32], polystyrene beads [33,34], and pegylated gold nanospheres [35,36]. However, the understanding of lipoproteins mesoscale properties (number density, rigidity, stiffness, curvature) and their interaction with other extracellular nanoparticles are still poorly understood and largely overlooked, although necessary to fulfill their clinical translation promises and to open new perspectives in bio-nanotechnology [14, 37–39]. Therefore, versatile methods allowing for the characterization of the mesoscale properties of native and engineered lipoproteins would be transformative for this research area.

Recently, citrate-capped gold nanoparticles (hereafter referred to as AuNPs) have been successfully implemented to probe mesoscale properties of synthetic and extracellular vesicles. Specifically, the spontaneous clustering of AuNPs on the vesicles [40], triggered by the substitution of the citrate molecules capping the AuNPs by phospholipids from the outer leaflet of the vesicle membrane [41,42], and the related redshift of the AuNP plasmonic signature, have been exploited as a colorimetric assay to determine the number density [43], the stiffness, and the purity of the vesicle samples [44].

In this work, sparked by the hypothesis that the phospholipid monolayer which delimits lipoproteins might interact with the AuNPs as the outer phospholipid leaflet of the vesicle membrane does, we explore for the first time the interaction of AuNPs with lipoproteins.

2. Material and methods

2.1. Lipoprotein standards

HDL, LDL, and VLDL standards were acquired from MyBioSource Inc. (San Diego, CA). IDL standards were acquired from LifeSpan Biosciences Inc. (Seattle, WA). Chylomicron standards were acquired from Biovision Inc. (Waltham, MA). Lipoproteins were characterized as reported in Section S2 of the Supporting Materials, aliquoted, and stored according to the manufacturer datasheet until further use. Lipoprotein standard characterization included Nanoparticle Tracking Analysis (NTA), Dynamic Light Scattering (DLS)l, pH determination, Western Blot (WB) versus specific apolipoproteins, and protein and lipid content determination using bicinchoninic acid (BCA) and sulfo-phospho-vanillin assays, respectively (Fig. S2).

2.2. Turkevich-Frens gold nanoparticles

Spherical, 16–18 nm citrate-capped gold nanoparticles (AuNPs) were synthesized following the citrate reduction approach first described by Turkevich et al. [45] (see also section S1) and characterized by UV–Vis spectroscopy and DLS (Fig. S1).

2.3. Gold Nanoplasmonics of lipoprotein standards: sample preparation

A fixed amount (250 μL, pH 6.9) of 6 nM AuNPs was challenged with a fixed amount (10 μL, pH 7.0) of 0.16 nM LP standards (Chylomicrons, VLDLs, LDLs, IDLs, and HDLs) at 25 °C. Samples were further diluted before analysis using 225 μL of Milli-Q water +25 μL of PBS 1x (pH 7.4) to enhance the interaction of AuNPs and lipoproteins (final volume = 500 μL). To detect the evolution of AuNP-lipoprotein aggregation, UV–vis spectra were collected at 25 °C, at different time points (T = 0, 5, 10, and 15 min).

2.4. Gold Nanoplasmonics of HDL: sample preparation

A fixed amount (250 μL, pH 6.9) of 6 nM AuNPs was challenged with a fixed amount (10 μL, pH 7.0) of HDL standards at variable concentrations (0.15 μM - 1.5 pM) and diluted in Milli-Q water (final volume = 500 μL). The final AuNP/HDL molar ratio (χ) ranged between $10^{-3} < \chi < 10^5$. All the measurements involving HDLs were performed in these conditions if not differently specified. Further details on characterization methods are given in Supplementary Material.

3. Results and discussion

3.1. AuNP-lipoprotein nanoplasmonics

AuNPs were mixed with lipoproteins and analyzed through UV–Vis spectroscopy to check variations of the plasmonic absorption band of AuNPs. Fig. 2 reports the UV–Vis spectra of AuNP-lipoprotein samples collected 15 min after mixing.

A first inspection of the UV–Vis spectra indicates that the plasmonic properties of the colloidally stable AuNP dispersion (Fig. 2, black profile) change upon interaction with lipoproteins, as suggested by the broadening of the LSPR peak (whose maximum is located at $\lambda = 522$ nm for pristine AuNPs) and eventually by the occurrence of a secondary redshifted plasmon absorption. This modification of the AuNP plasmonic properties is consistent with plasmon-plasmon coupling due to their aggregation triggered by the lipoproteins.

Indeed, Fig. 2 shows that the AuNP aggregation extent depends on the lipoprotein class (milder for chylomicrons, Fig. 2 blue spectrum, very
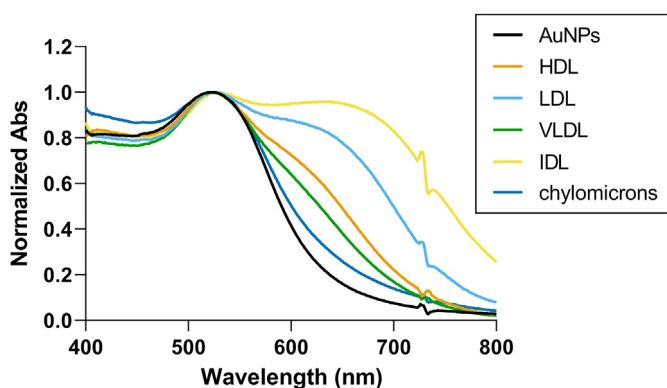
Fig. 2. Interaction between AuNPs and LPs through UV-Vis spectroscopy. 6 nM AuNPs were challenged with 0.16 nM of lipoprotein standards (Chylomicrons, VLDLs, LDLs, IDLs, and HDLs, $\chi = 37.5$) in the presence of PBS. UV-Vis spectra of the samples were collected after 15 min of incubation to visualize the broadening of the plasmonic absorption or the occurrence of a second red-shifted band. Note: the spikes around 720 nm are artifacts due to the spectrophotometer switching the visible lamp to the NIR lamp.

marked for IDLs, Fig. 2 yellow spectrum), as the entity of both the redshift and the broadening of the LSPR peak changes with it. Interestingly, the broadening of the LSPR peak and red shifting of the plasmon absorption band of AuNPs follows an unexpected order, that is: chylomicrons < VLDL < HDL < LDL < IDL. This order does not directly relate to lipoprotein size or density, and may therefore be influenced by other parameters, such as i) particle surface area ii) particle surface charge, or iii) particle mechanical properties, which was recently shown to differentially correlate with lipoprotein class [14,37]. Most likely, the interaction between lipoproteins and AuNPs is dictated by the simultaneous interplay of several - if not all - these physicochemical parameters, but to better understand their contribution, each of these parameters should be specifically studied. Nevertheless, the finding that lipoprotein class can be distinguished based on the plasmonic red shift of AuNPs is a promising indication that AuNP nanoplasmonics can be an accessible yet powerful tool to characterize lipoprotein physicochemical properties, paving the way for further analytical developments.

Finally, from a more fundamental perspective, this finding provides a positive experimental indication of our working hypothesis (see the introduction section) on the analogies between the interaction of AuNPs with lipoproteins and the interaction of AuNPs and (biogenic and synthetic) vesicles [41,46,47].

3.2. (Further investigation of) AuNP-HDL nanoplasmonics

Among the known lipoproteins, HDLs are the smallest (7–10 nm) and densest (1019 - 1210 g/ml) and are responsible for the removal and transport of cholesterol and triglycerides from peripheral tissues to the liver, to the surrenal glands and the gonads.

Despite their physiological role has been deeply investigated and they are regularly used as molecular biomarkers, their mesoscale and interfacial properties - such as stiffness [14,37] and interaction with other synthetic nanoparticles - have been scarcely investigated [31–36,39], also because their very small size still poses severe challenges even to the most advanced microscopy techniques, including cryo-EM, in liquid-AFM and ultramicroscopy.

Therefore, we opted for further investigating the interaction between AuNPs and HDLs, in search of possible/promising results towards its translation to an analytical technique.

In particular, we decided to investigate the interaction across several (order of magnitude of) AuNP/HDL molar ratios (χ). The redshift of the AuNP LSPR peak here was correlated with the AuNP/HDL molar ratio (χ) and conveniently expressed using the Percentage Aggregation Index (AI

%), a numerical descriptor of the UV–Vis spectral variations used to describe the aggregation state of AuNP in solution. AI% is inversely proportional to AuNP aggregation: the higher the AI%, the lower the aggregation, and vice-versa [43].

A fixed amount of AuNPs was challenged with variable amounts of HDL, the UV–Vis spectra were collected after 15', and the AI% was calculated (Fig. 3). Fig. 3A reports the AI% of the tested samples as a function of the AuNP/HDL molar ratio (χ).

For $10^5 < \chi < 10^2$, AI% is almost constant, and the dispersion color is identical to the original AuNP dispersion (red, Fig. 3B and Fig. S3); in line with this visual observation, the respective UV–Vis spectra are superimposable to that of pristine AuNPs (Fig. 3B, green spectrum, and Fig. S3). This suggests that, at this stage, the interaction between AuNPs and HDLs is limited, probably due to the HDL number being too low to trigger significant AuNP aggregation.

For $1 < \chi < 10$ samples show an intense aggregation of AuNPs, with a broadening of AuNP LSPR peak and a related color change of the AuNP solution (deep purple, Fig. 3B and Fig. S3). A selected example of such samples - corresponding to $\chi = 10$ - is given in Fig. 3B (yellow spectrum). It is worth noting that these colloidal dispersions did not lose their colloidal stability, and proved to be kinetically stable for the entire duration of the measurements performed (including the ones presented in the next sections).

On the contrary, for $\chi < 1$, the dispersion consists of a hazy particulate that settles in the cuvette within minutes. A selected example of the UV–Vis spectra of such samples is given in Fig. 3B (orange spectrum), showing a minimal broadening of the AuNP LSPR peak and a consistent raising of the absorbance at $650\ nm < \lambda < 800\ nm$. This phenomenon is usually caused by the loss of colloidal stability of the nanoparticles, leading to the uncontrolled formation and flocculation of micrometer-sized aggregates. The formation of such unstable aggregates is also suggested by the increase of absorbance in the 650–800 nm region of the UV–Vis spectrum (Fig. 3B, orange spectrum) due to light scattering events. Interestingly, similar aggregation phenomena have already been observed when challenging synthetic and biogenic lipid vesicles with AuNPs and related to either the physicochemical characteristics of the vesicles (stiffness in particular) or AuNP/lipid vesicle molar ratio. Both phenomena are investigated here for the first time on HDLs and suggest that AuNP-HDL interaction may be similar to AuNP-lipid vesicle one.

Very interestingly, a "spike" in the AI% located at $\chi = 1$ separates the two aggregation regimes at which AuNPs interact with HDLs, representing a "watershed" at which none of the two aggregative phenomena seems to prevail (Fig. 3A yellow dot and inset, Fig. 3B yellow line). The formation of this spike in the region of $\chi = 1$ proves to be rather robust, as its occurrence is reproducible and shows a fair (<20%) AuNP-related batch-to-batch variation.

Finally, it is interesting to notice that the AI% does not clearly describe the complexity of AuNP-HDL interaction, as it fails to distinguish the stable, controlled AuNP aggregation observed at $1 < \chi < 10$ from unstable flocculation and precipitation observed for AuNP/HDL molar ratios $\chi > 1$. Indeed AI% have similar values in both cases, but the UV–Vis and visual sample readout are extremely different (Fig. S3).

To shed light on this aspect, we further investigated two selected experimental conditions, one characterized by colloidally stable AuNP-HDL hybrid systems, and the other one by flocculation.

3.3. Further assessment of AuNP-HDL interaction

To better characterize the interaction between AuNPs and HDLs, we tracked with DLS the colloidal stability of the hybrid AuNP-HDL systems over time. We chose AuNP/HDL molar ratios $\chi = 10$ and $\chi = 10^{-3}$, which feature the lowest AI% among the tested conditions, as the representative samples of stable and unstable colloidal dispersions, respectively. The normalized measured autocorrelation functions analyzed through a CONTIN algorithm, a characteristic fitting model employed for polydisperse colloids, are reported in Fig. 4. When the amount AuNPs is in
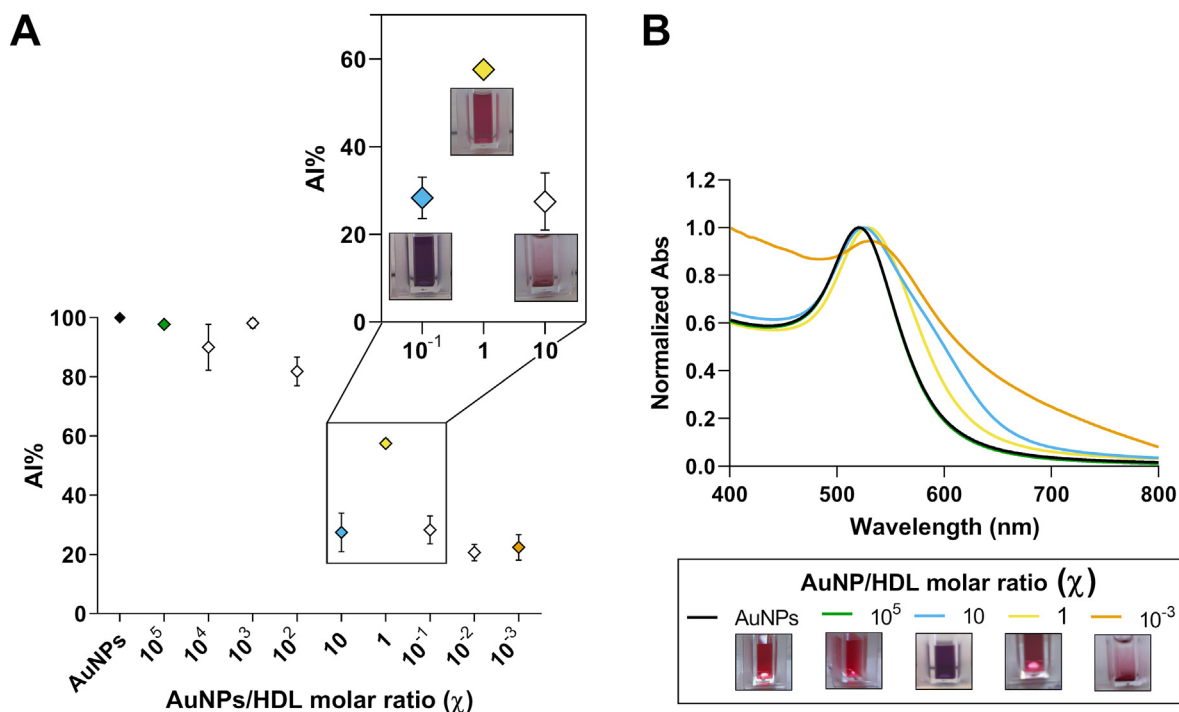
Fig. 3. Interaction between AuNPs and HDLs through UV-Vis spectroscopy. A) AI% extrapolated from the UV-Vis spectra of AuNP-HDL samples. The AI% displays a descending sigmoidal trend following the AuNP/HDL molar ratio χ, with a spike located at $\chi = 1$ that separates two different AuNP aggregation regimes. Such regimes are hardly distinguishable in terms of AI% but can be inferred both from UV-Vis spectra and by the naked eye. Plotted values refer to the average AI% of 3 physical replicates +/- SD. Colored dots refer to the AI% extrapolated from the respective spectra shown in panel B. The inset magnifies the AuNP/HDL molar ratio χ values around which the switch between the two different aggregation phenomena (stable and unstable aggregation) occurs. B) UV-Vis spectra of selected AuNP-HDL samples, suggesting AuNPs and HDL interaction change upon the modification of the AuNP/HDL molar ratio χ. For $\chi > 10$, no appreciable aggregation between AuNPs and HDLs was observed (green spectrum and related inset, $\chi = 10^5$). Stable AuNP aggregation was observed for $1 < \chi < 10$ (cyan spectrum and related inset, $\chi = 10$), while AuNP flocculation and precipitation were observed for AuNP/HDL molar ratio $\chi < 1$ (orange spectrum and related inset, $\chi = 10^{-3}$). Such different aggregation regimes are separated by an equilibrium point (yellow spectrum and related inset, $\chi = 1$), at which AuNPs mildly interact with HDLs.
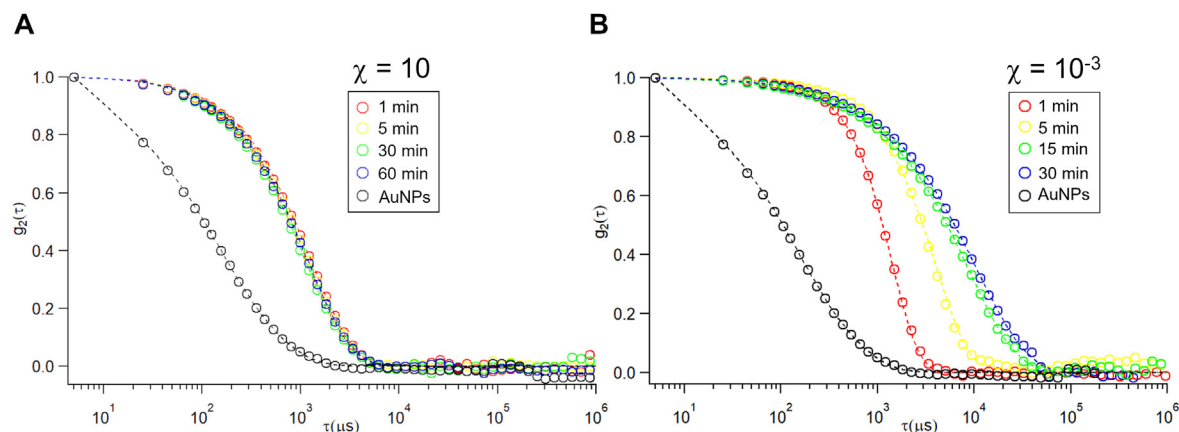

Fig. 4. Time-resolved DLS of selected AuNP-HDL samples to monitor the formation and evolution of AuNP-HDL hybrids over time. A) Time evolution of the DLS curves of the AuNPs-HDL sample corresponding to an $\chi = 10$. The curves are compatible with the formation of aggregates with a size of ~ 300 nm, which remains colloidally stable. B) Time evolution of the DLS curves of the AuNPs-HDL sample corresponding to $\chi = 10^{-3}$. The curves are compatible with the formation of aggregates that progressively grows to the size of several micrometers, ultimately leading to their precipitation.

excess with respect to the HDLs ($\chi = 10$), the incubation leads to the immediate formation of colloidally stable hybrids of about 300 nm, which are significantly larger compared to pristine AuNPs and HDLs (Fig. 4A, see SI for AuNPs and HDL characterization). On the other hand, an excess of HDLs ($\chi = 10^{-3}$) leads to an evident shift in the decay times of the autocorrelation function, evidencing the formation of progressively larger HDL-AuNP hybrids, and eventually leading to the sedimentation, always observed for $\chi < 1$ (Fig. 4B).

Further information is given by ζ-potential measurements. In presence of an excess of AuNPs ($\chi = 10$), the hybrids have a ζ-potential of -34 ± 4 mV, very similar to the ζ-potential of pristine AuNPs and compatible with the formation of AuNP-decorated HDLs, thus ensuring electrostatic stabilization. On the other hand, hybrids obtained in presence of an excess of HDLs ($\chi = 10^{-3}$) are characterized by a much higher ζ-potential (-15 ± 3 mV), explaining their lower stability, and highlighting the formation of HDL-decorated AuNPs. Interestingly, this dual

regime has been already described for other inorganic versus lipidic nanoparticle interacting systems. For instance, several studies showed that the adhesion of charged inorganic nanoparticles on the surface of zwitterionic liposomes dramatically affects the colloidal stability of the system. For example, charged AuNPs can charge the external phospholipid leaflet of the liposome and contribute to electrostatic stabilization, forming kinetically stable complexes. However, this electrostatic stability is only gained when enough AuNPs are bound to the liposomes. Otherwise, if the number of AuNPs is lower, the colloidal dispersion is instantly destabilized by Van der Waals attractions between AuNP-vesicle hybrids [42,48–51]. To gain further information on the AuNP/HDL interaction occurring in the case of stable and unstable hybrid systems, we investigated the structure and morphology of the representative samples (χ =10 and $\chi = 10^{-3}$) using cryo-EM. Representative images are reported in Fig. 5. As expected, [37] HDLs are scarcely detectable due to i) intrinsically low density and small size, which hamper their visualization with conventional imaging techniques, and ii) the high contrast of AuNPs. Nevertheless, the spatial arrangement of AuNPs resulting from the interaction with HDLs provides relevant structural information on AuNP-HDL hybrids. Fig. 5A displays representative Cryo-EM images obtained by incubating AuNPs and HDLs at an AuNP/HDL molar ratio χ =10 (see Fig. S4 for more micrographs). As shown, the interaction leads to the formation of AuNP clusters, with AuNPs in direct contact with each other. This is also highlighted by the measurement of the average interparticle space between AuNP (Fig. 5C, ~ 18 nm), which almost matches AuNP diameter (16–18 nm). Moreover, the morphology of such clusters is in line with the nanoplasmonic variations observed in UV–vis spectroscopy measurements (Fig. 3). On the other hand, for $\chi = 10^{-3}$ (Fig. 5B and Fig. S5), the AuNP/HDL interaction leads to the formation of larger micron-sized suprastructures characterized by a significantly higher average interparticle spacing (shown in Fig. 5D, ~ 26 nm), just partially affecting the plasmonic features of AuNPs (hence, the little variation in the color solution, Fig. 3B and Fig. S3).

Although cryo-EM imaging provides extremely precise structural information about single or small groups of AuNP-HDL hybrids, it fails to provide such information at the ensemble level. To fill this gap, the hybrid structure of AUNP-HDL hybrids was further characterized by SAXS. SAXS measurements allow obtaining ensemble-averaged information on the structural changes induced by the interaction of the AuNPs with the HDLs, avoiding the presence of any possible artifacts originating from the cryo-EM sample preparation. As for cryo-EM, due to their low electron density, the HDL contribution to the scattering signal can be neglected, and only AuNPs are detected. As such, any variation observed in the spectra with respect to the pristine AuNP dispersion is ascribed to the structural rearrangement induced by the interaction with HDL. Fig. 6 displays the absolute scattering intensity I(q) as a function of the scattering vector q obtained from dilute dispersions of AuNPs in the presence (Fig. 6 blue line for $\chi = 10$ and green line for $\chi = 10^{-3}$) or the absence (Fig. 6, red line) of HDLs.

The SAXS profile of the pristine AuNP dispersion was analyzed through a polydisperse spherical particle model [52] (see Supporting Materials). For the hybrid samples, we first extrapolated the mean interparticle distance using a model-free analysis of the structure factor S(Q), extracted as described in SI, section S2.5. The appearance of structure peaks is attributed to the formation of AuNP clusters. The Q position of the peaks is related to the AuNP-AuNP mean distance within the cluster (d=2π/Q). In the case of an AuNP/HDL molar ratio $\chi = 10$ (Fig. 6 blue line), we obtained a center-to-center spacing of 15 nm. This distance, almost matching the AuNP diameter, highlights that the particles are in contact with each other, as observed (Fig. 5A and S4) and measured (Fig. 5C) in the corresponding cryo-EM micrographs, (Fig. 5C), . On the other hand, in the case of $\chi = 10^{-3}$ (Fig. 6, green line), the evaluated interparticle distance is 26 nm, again reflecting the higher average spacing detected and observed with cryo-EM (Fig. 5B and D, and Fig. S5).

Further confirmations of the structure of the hybrid complexes were obtained by analyzing the SAXS profiles with the Sticky Hard Spheres
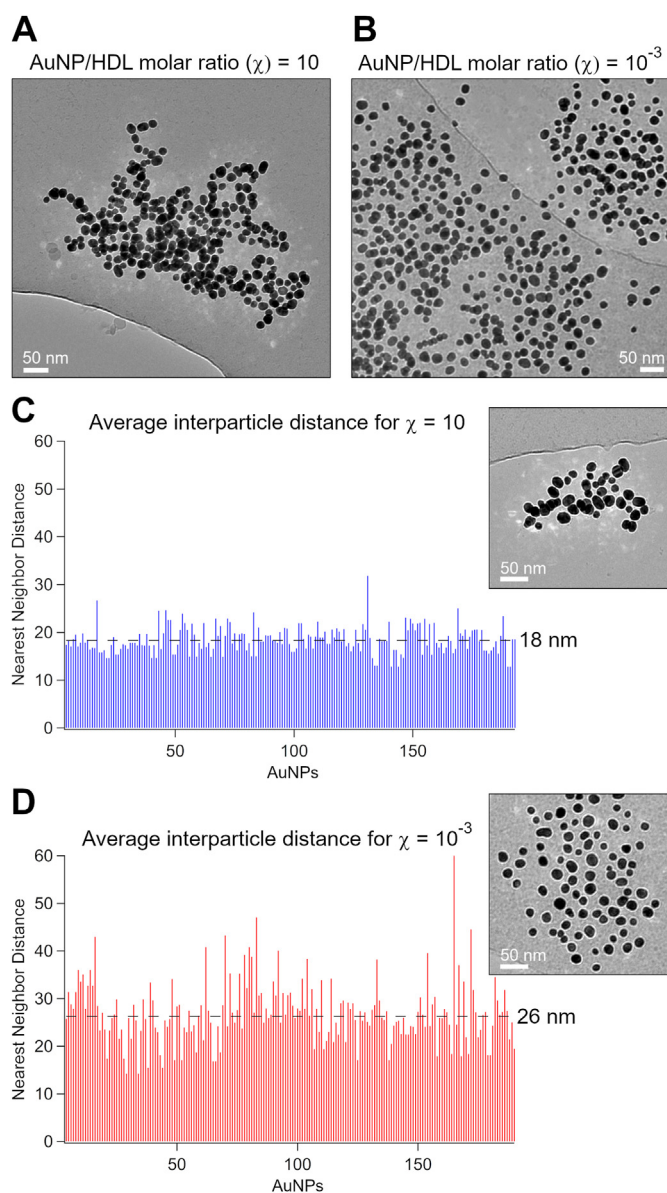
A
AuNP/HDL molar ratio (χ) = 10

B
AuNP/HDL molar ratio (χ) = 10^{-3}

C
Average interparticle distance for $\chi = 10$

18 nm

D
Average interparticle distance for $\chi = 10^{-3}$

26 nm

Fig. 5. Cryo-EM imaging of AuNP-HDL hybrids. A) Representative Cryo-EM image of the AuNP-HDL sample corresponding to an $\chi = 10$. In these conditions, the interaction of AuNPs with HDLs leads to the formation of AuNP clusters, with AuNPs in direct contact with each other. B) Representative Cryo-EM image of the AuNP-HDL sample corresponding to $\chi = 10^{-3}$. In these conditions, the interaction of AuNPs with HDLs leads to the formation of micron-sized suprastructures characterized by a visibly larger AuNP interparticle spacing. C) The interparticle spacing of 200 representative AuNPs in AuNP-HDL sample corresponding to $\chi = 10$ is here reported, and the average interparticle spacing highlighted (black dashed line). D) The interparticle spacing of 200 representative AuNPs in AuNP-HDL sample corresponding to $\chi = 10^{-3}$ is here plotted, and the average interparticle spacing highlighted (black dashed line).

model, a theoretical model for hard particles interacting with an attractive short-range potential [53–55]. The numerical analysis was performed with the SASview software package, keeping the particle size extrapolated from the SAXS fit of the AuNP profile constant (see SM for the full SAXS analysis). The effective hard sphere radius extrapolated for $\chi = 10$ and $\chi = 10^{-3}$ are 8.6 $\pm$ 0.3 nm and 14.7 $\pm$ 0.5 nm, respectively. Such results are in line with the ones obtained through the model-free analysis of the S(Q).

Interestingly, the average AuNP-AuNP spacing obtained for AuNP/ HDL molar ratio $\chi = 10^{-3}$ (approximately 6 nm) fits the average size of an
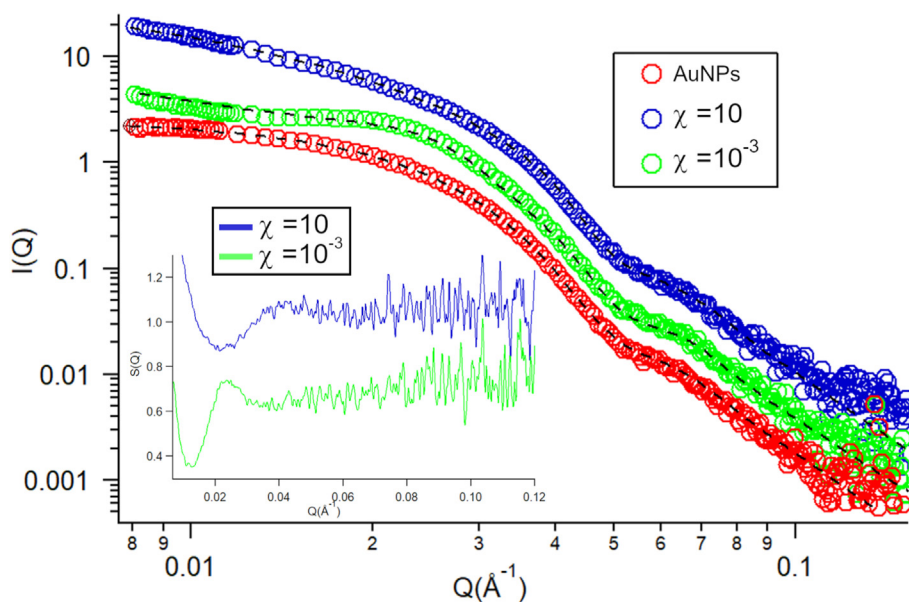
Fig. 6. SAXS analysis of pristine AuNPs and AuNP-HDL samples. The SAXS profiles of pristine AuNPs (red circles), the AuNP-HDL sample with an AuNP/HDL molar ratio $\chi = 10$ (blue circles), and the one with an AuNP/HDL molar ratio $\chi = 10^{-3}$ (green circles) are reported. The black dashed lines represent the fits by the SHS model. The inset reports the intensity peaks of the S(Q) profiles of the AuNP-HDL sample with $\chi = 10$ (blue line) and AuNP-HDL sample with $\chi = 10^{-3}$ (green line), respectively.

HDL (7–10 nm). This aspect - together with the interparticle distance data provided by cryoEM analysis - suggests that HDLs may keep their integrity upon interacting with the AuNP surface, with no major structural disruption occurring. Therefore, after their adhesion to the AuNP surface, HDLs may act as bridges between adjacent AuNPs, eventually leading to the formation of the micron-sized structures highlighted by DLS and by the phase separation noticed during UV–Vis measurements. This finding is supported by works reporting the formation of a corona of intact HDLs on the surface of co-polymeric [31] and silica NPs [32], but is also in contrast with reports showing the disintegration of the lipoproteins and the formation of a loose lipid corona upon LP interaction with PEGylated gold nanoparticles [35] and polystyrene ones [33]. Also, it might be possible that HDLs disintegrate and cover the AuNPs until surface saturation is reached, with subsequent adsorption of an additional layer of intact HDLs occurring [33]. Nevertheless our findings, here reported for the first time for citrate-capped gold nanoparticles, further corroborate the importance of NP features (material, capping agents, surface charge etc.) in determining the outcome of NP-HDL interaction.

Moreover, the experimental data suggest that the colloidal stability of the AuNPs-HDL hybrids, as well as their plasmonic variations and cluster morphology, are strictly related to the AuNPs/HDL number ratio. For high AuNP concentrations, AuNPs aggregate on the HDL surface, forming kinetically stable complexes and provoking the change of the color of the dispersion from red to purple/blue, with optical variations directly connected to the HDL concentration. On the other hand, a high amount of HDLs triggers an aggregation phenomenon that forms HDL-decorated AuNPs, eventually destabilizing the dispersion. This difference in the colloidal properties of the dispersion could be used to extrapolate quantitative information from unknown lipoprotein samples.

4. Conclusions

In this work, the interaction of citrate-capped gold nanoparticles (AuNPs) with lipoproteins has been investigated for the first time. It channels with and contributes to the very recent efforts in expanding to lipoproteins the understanding of the interaction between synthetic and biogenic nanomaterials, motivated by both medical [24–30] and technical [31–36] envisioned very promising applications [27–29].

By combining UV–vis spectroscopy, cryo-EM, SAXS, and DLS we were able to show that: (i) lipoproteins trigger/template AuNP aggregation and a related plasmonic redshift and that (ii) such interaction and its plasmonic signature are sensitive to the different lipoprotein classes. In addition, it was found that (iii) for HDLs, AuNP aggregation falls into two different regimes, depending on the AuNP/lipoprotein molar ratio, characterized by different colloidal stability of the formed AuNP-lipoprotein mesostructures (summarized in Fig. 7). Very interestingly, the regime sharply switches at an AuNP/HDL molar ratio equal to 1.

Still, several aspects remain to be elucidated, providing material for future discussions on the AuNP-biogenic nanoparticle interaction topic: among the others (i) the unraveling of the molecular mechanism behind AuNP-HDL interaction and (ii) if and to what extent it applies to the other classes of lipoproteins, or, in other words how lipoprotein composition, size, stiffness, and surface charge modulate the interaction with AuNPs, and finally (iii) the role of the surface properties of AuNPs (e.g. surface charge, capping agents, presence or absence of a protein corona etc.) in the modulation/modification of AuNP-LP interaction. Nevertheless, the findings candidate citrate-capped AuNP nanoplasmonics as an innovative
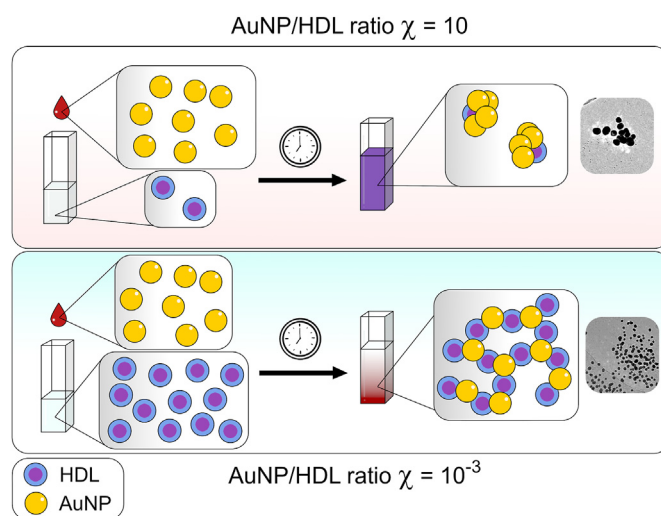

Fig. 7. Schematic representation of the proposed interaction mechanism between AuNPs and HDL in the two limit cases analyzed. The outcome of the interaction depends on the AuNP/HDL molar ratio χ. For $\chi = 10$, AuNP/HDL hybrids evolve in single, kinetically stable clusters of AuNPs of a few hundreds of nanometers. For $\chi = 10^{-3}$, AuNP/HDL hybrids flocculate into micron-sized suprastructures where HDLs seem to act as a bridge between AuNPs.

analytical method to evaluate lipoprotein formulations at the mesoscale, including titration, adding new valuable information in the realization of lipoprotein–inorganic nanoparticle hybrid systems and, on a wider perspective, expand current knowledge of the AuNP-extracellular nanoparticle interface.

Funding

Author contributions

Conceptualization: P.B., A.Z. Data curation: J.C., R.F., A.Z. Funding acquisition: P.B., D.B., Investigation: M.B., J.C., R.F., A.Z. Methodology: P.B., J.C., R.F., A.Z. Project administration: P.B., D.B, Resources; P.B., D.B. Supervision: P.B., A.Z. Visualization; J.C., R.F., A.Z. Writing - original draft: P.B, J.C., R.F., A.Z. Writing - review & editing: all authors.

Declaration of competing interest

The authors declare that they have no known competing financial interests or personal relationships that could have appeared to influence the work reported in this paper.

Data availability

Data will be made available on request.

Appendix A. Supplementary data

Supplementary data to this article can be found online at https://doi.org/10.1016/j.jciso.2023.100088.

References

[1] H. Tjalsma, A. Bolhuis, J.D.H. Jongbloed, S. Bron, J.M. van Dijl, Signal peptide-dependent protein transport in Bacillus subtilis: a genome-based survey of the secretome, Microbiol. Mol. Biol. Rev. 64 (3) (2000) 515–547, https://doi.org/10.1128/mmbr.64.3.515-547.2000.

[2] G. van Niel, G. D'Angelo, G. Raposo, Shedding light on the cell biology of extracellular vesicles, Nat. Rev. Mol. Cell Biol. 19 (4) (2018) 213–228, https://doi.org/10.1038/nrm.2017.125.

[3] S.L.N. Maas, X.O. Breakefield, A.M. Weaver, Extracellular vesicles: unique intercellular delivery vehicles, Trends Cell Biol. 27 (3) (2017) 172–188, https://doi.org/10.1016/j.tcb.2016.11.003.

[4] N. Díaz-Garrido, J. Badia, L. Baldomà, Microbiota-derived extracellular vesicles in interkingdom communication in the gut, J. Extracell. Vesicles 10 (13) (2021), https://doi.org/10.1002/jev2.12161.

[5] R. Kalluri, V.S. LeBleu, The biology, function, and biomedical applications of exosomes, Science 367 (6478) (2020), https://doi.org/10.1126/science.aau6977.

[6] L. Paolini, S. Federici, G. Consoli, D. Arceri, A. Radeghieri, I. Alessandri, P. Bergese, Fourier-transform Infrared (FT-IR) spectroscopy fingerprints subpopulations of extracellular vesicles of different sizes and cellular origin, J. Extracell. Vesicles 9 (1) (2020), 1741174, https://doi.org/10.1080/20013078.2020.1741174.

[7] Y. Zhang, B.P. Orner, Self-assembly in the ferritin nano-cage protein superfamily, Int. J. Mol. Sci. 12 (8) (2011) 5406–5421, https://doi.org/10.3390/ijms12085406.

[8] K. Li, R.S. Rodosthenous, F. Kashanchi, T. Gingeras, S.J. Gould, L.S. Kuo, P. Kurre, H. Lee, J.N. Leonard, H. Liu, T.B. Lombo, S. Momma, J.P. Nolan, M.J. Ochocinska, D.M. Pegtel, Y. Sadovsky, F. Sánchez-Madrid, K.M. Valdes, K.C. Vickers, A.M. Weaver, Advances, challenges, and opportunities in extracellular RNA biology: insights from the NIH exRNA Strategic Workshop, JCI Insight 3 (7) (2018), https://doi.org/10.1172/jci.insight.98942.

[9] A.V. Vlassov, S. Magdaleno, R. Setterquist, R. Conrad, Exosomes: current knowledge of their composition, biological functions, and diagnostic and therapeutic potentials, Biochim. Biophys. Acta Gen. Subj. 1820 (7) (2012) 940–948, https://doi.org/10.1016/j.bbagen.2012.03.017.

[10] G. Raposo, W. Stoorvogel, Extracellular vesicles: exosomes, microvesicles, and friends, J. Cell Biol. 200 (4) (2013) 373–383, https://doi.org/10.1083/jcb.201211138.

[11] A. Rai, D.W. Greening, R. Xu, M. Chen, W. Suwakulsiri, R.J. Simpson, Secreted midbody remnants are a class of extracellular vesicles molecularly distinct from exosomes and microparticles, Communications Biology 4 (1) (2021), https://doi.org/10.1038/s42003-021-01882-z.

[12] S. Raut, J.-L. Dasseux, N.A. Sabnis, L. Mooberry, A. Lacko, Lipoproteins for therapeutic delivery: recent advances and future opportunities, Ther. Deliv. 9 (4) (2018) 257–268, https://doi.org/10.4155/tde-2017-0122.

[13] P.H.D. Nguyen, A.H. Le, J.S.Q. Pek, T.T. Pham, M.K. Jayasinghe, D.V. Do, C.D. Phung, M.T.N. Le, Extracellular vesicles and lipoproteins – smart messengers of blood cells in the circulation, Journal of Extracellular Biology 1 (7) (2022), https://doi.org/10.1002/jex2.49.

[14] M.C. Piontek, W.H. Roos, Lipoprotein particles exhibit distinct mechanical properties, Journal of Extracellular Biology 1 (12) (2022), https://doi.org/10.1002/jex2.68.

[15] J. Vekic, A. Zeljkovic, K. Al Rasadi, M. Cesur, J. Silva-Nunes, A.P. Stoian, M. Rizzo, A new look at novel cardiovascular risk biomarkers: the role of atherogenic lipoproteins and innovative antidiabetic therapies, Metabolites 12 (2) (2022) 108, https://doi.org/10.3390/metabo12020108.

[16] J.L. Sanchez-Quesada, Modified low-density lipoproteins as biomarkers in diabetes and metabolic syndrome, Front. Biosci. 23 (4) (2018) 1220–1240, https://doi.org/10.2741/4640.

[17] Y. Kaiser, M. Daghem, E. Tzolos, M.N. Meah, M.K. Doris, A.J. Moss, J. Kwiecinski, J. Kroon, N.S. Nurmohamed, P. van der Harst, P.D. Adamson, M.C. Williams, D. Dey, D.E. Newby, E.S.G. Stroes, K.H. Zheng, M.R. Dweck, Association of lipoprotein(a) with atherosclerotic plaque progression, J. Am. Coll. Cardiol. 79 (3) (2022) 223–233, https://doi.org/10.1016/j.jacc.2021.10.044.

[18] X. Zhang, G. Huang, Synthetic lipoprotein as nano-material vehicle in the targeted drug delivery, Drug Deliv. 24 (2) (2017) 16–21, https://doi.org/10.1080/10717544.2017.1384518.

[19] L. Cui, Y. Wang, M. Liang, X. Chu, S. Fu, C. Gao, Q. Liu, W. Gong, M. Yang, Z. Li, L. Yu, C. Yang, Z. Su, X. Xie, Y. Yang, C. Gao, Dual-modified natural high density lipoprotein particles for systemic glioma-targeting drug delivery, Drug Deliv. 25 (1) (2018) 1865–1876, https://doi.org/10.1080/10717544.2018.1519002.

[20] X. Ma, Q. Song, X. Gao, Reconstituted high-density lipoproteins: novel biomimetic nanocarriers for drug delivery, Acta Pharm. Sin. B 8 (1) (2018) 51–63, https://doi.org/10.1016/j.apsb.2017.11.006 [online].

[21] P. Kadiyala, D. Li, F.M. Nuñez, D. Altshuler, R. Doherty, R. Kuai, M. Yu, N. Kamran, M. Edwards, J.J. Moon, P.R. Lowenstein, M.G. Castro, A. Schwendeman, High-density lipoprotein-mimicking nanodiscs for chemo-immunotherapy against glioblastoma multiforme, ACS Nano 13 (2) (2019) 1365–1384, https://doi.org/10.1021/acsnano.8b06842.

[22] R. Kuai, X. Sun, W. Yuan, L.J. Ochyl, Y. Xu, A. Hassani Najafabadi, L. Scheetz, M.-Z. Yu, I. Balwani, A. Schwendeman, J.J. Moon, Dual TLR agonist nanodiscs as a strong adjuvant system for vaccines and immunotherapy, J. Contr. Release 282 (2018) 131–139, https://doi.org/10.1016/j.jconrel.2018.04.041.

[23] K.-H. Cho, Enhanced delivery of rapamycin by V156K-apoA-I high-density lipoprotein inhibits cellular proatherogenic effects and senescence and promotes tissue regeneration, The Journals of Gerontology Series A: Biological Sciences and Medical Sciences 66A (12) (2011) 1274–1285, https://doi.org/10.1093/gerona/glr169.

[24] W. Ngo, J.L.Y. Wu, Z.P. Lin, Y. Zhang, B. Bussin, A. Granda Farias, A.M. Syed, K. Chan, A. Habsid, J. Moffat, W.C.W. Chan, Identifying cell receptors for the nanoparticle protein corona using genome screens, Nat. Chem. Biol. 18 (9) (2022) 1023–1031, https://doi.org/10.1038/s41589-022-01093-5 [online].

[25] Mongkhol Prawatborisut, J. Oberländer, S. Jiang, R. Graf, Y. Avlasevich, S. Morsbach, D. Crespy, Volker Mailänder, K. Landfester, Temperature-responsive nanoparticles enable specific binding of apolipoproteins from human, Plasma 18 (3) (2021) 2103138, https://doi.org/10.1002/smll.202103138, 2103138.

[26] E. Li, Joshua U-Jin Cheah, Patricia Khee, Chee Soo, J. Chen, Gold nanorods coated with apolipoprotein, E Protein Corona for Drug Delivery 2 (10) (2019) 6220–6229, https://doi.org/10.1021/acsanm.9b01196.

[27] Y. Peng, Y. Cong, Y. Lei, F. Sun, M. Xu, J. Zhang, L. Fang, H. Hong, T. Cai, Transforming passive into active: multimodal pheophytin-based carbon dots customize protein, Corona to Target Metastatic Breast Cancer 11 (8) (2022) 2102270, https://doi.org/10.1002/adhm.202102270, 2102270.

[28] Z. Wang, H. Cheng, Y. Sheng, Z. Chen, X. Zhu, J. Ren, X. Zhang, L. Lv, H. Zhang, J. Zhou, Y. Ding, Biofunctionalized Graphene Oxide Nanosheet for Amplifying Antitumor Therapy: Multimodal High Drug Encapsulation, Prolonged Hyperthermal Window, and Deep-Site Burst Drug Release, Biomaterials, 2022, 121629, https://doi.org/10.1016/j.biomaterials.2022.121629 [online] 287.

[29] R. Dal Magro, B. Albertini, S. Beretta, R. Rigolio, E. Donzelli, A. Chiorazzi, M. Ricci, P. Blasi, G. Sancini, Artificial apolipoprotein corona enables nanoparticle brain targeting, Nanomed. Nanotechnol. Biol. Med. 14 (2) (2018) 429–438, https://doi.org/10.1016/j.nano.2017.11.008 [online].

[30] D. Chen, N. Parayath, S. Ganesh, W. Wang, M. Amiji, The role of apolipoprotein- and vitronectin-enriched protein corona on lipid nanoparticles for in vivo targeted delivery and transfection of oligonucleotides in murine tumor models, Nanoscale 11 (40) (2019) 18806–18824, https://doi.org/10.1039/c9nr05788a.

[31] E. Hellstrand, I. Lynch, A. Andersson, T. Drakenberg, B. Dahlbäck, K.A. Dawson, S. Linse, T. Cedervall, Complete high-density lipoproteins in nanoparticle corona, FEBS J. 276 (12) (2009) 3372–3381, https://doi.org/10.1111/j.1742-4658.2009.07062.x.

[32] Nguyen Dang Nam and Sang Won Han, formation of high-density lipoprotein (HDL) coronas on silica nanoparticles occurs by adsorption of intact, HDL Particulates 37 (1) (2016) 3–4, https://doi.org/10.1002/bkcs.10622.

[33] J. Müller, D. Prozeller, A. Ghazaryan, M. Kokkinopoulou, V. Mailänder, S. Morsbach, K. Landfester, Beyond the Protein Corona – Lipids Matter for Biological Response of Nanocarriers, Acta Biomaterialia, 2018, pp. 420–431, https://doi.org/10.1016/j.actbio.2018.02.036 [online] 71.

[34] T. Lima, K. Bernfur, M. Vilanova, T. Cedervall, Understanding the lipid and protein corona formation on different sized polymeric nanoparticles, Sci. Rep. 10 (1) (2020), https://doi.org/10.1038/s41598-020-57943-6.

[35] S.H. Kim, C. Lee, G.J. Jang, S. Yoo, S. Lee, S.Y. Han, Understanding the biomolecular coronas of high-density lipoproteins on PEGylated Au nanoparticles: implication for lipid corona formation in the blood, ACS Appl. Nano Mater. 5 (2) (2022) 2018–2028, https://doi.org/10.1021/acsanm.1c03752.

[36] Gwi Yeong Jang, Ji Hoon Jeong, J.-H. Kang, W. Cho, Sang Won Han, Size dependence unveiling the adsorption interaction of high-density lipoprotein particles with PEGylated gold nanoparticles in biomolecular, Corona Formation 37 (32) (2021) 9755–9763, https://doi.org/10.1021/acs.langmuir.1c01182.

[37] A. Ridolfi, L. Conti, M. Brucale, R. Frigerio, J. Cardellini, A. Musicò, M. Romano, A. Zendrini, L. Polito, G. Bergamaschi, A. Gori, C. Montis, L. Barile, D. Berti, A. Radeghieri, P. Bergese, M. Cretich, Compositional profiling of EV-lipoprotein mixtures by AFM nanomechanical imaging, bioRxiv (2022), https://doi.org/10.1101/2022.07.19.500441.

[38] S. Busatto, Y. Yang, S.A. Walker, I. Davidovich, W.-H. Lin, L. Lewis-Tuffin, P.Z. Anastasiadis, J. Sarkaria, Y. Talmon, G. Wurtz, J. Wolfram, Brain metastases-derived extracellular vesicles induce binding and aggregation of low-density lipoprotein, J. Nanobiotechnol. 18 (1) (2020), https://doi.org/10.1186/s12951-020-00722-2.

[39] D.N. Trinh, M. Radlinskaite, J. Cheeseman, G. Kuhnle, H.M.I. Osborn, P. Meleady, D.I.R. Spencer, M.P. Monopoli, Biomolecular corona stability in association with plasma cholesterol level, Nanomaterials 12 (15) (2022) 2661, https://doi.org/10.3390/nano12152661.

[40] C. Montis, D. Maiolo, I. Alessandri, P. Bergese, D. Berti, Interaction of nanoparticles with lipid membranes: a multiscale perspective, Nanoscale 6 (12) (2014) 6452–6457, https://doi.org/10.1039/c4nr00838c.

[41] C. Montis, L. Caselli, F. Valle, A. Zendrini, F. Carlà, R. Schweins, M. Maccarini, P. Bergese, D. Berti, Shedding light on membrane-templated clustering of gold nanoparticles, J. Colloid Interface Sci. 573 (2020) 204–214, https://doi.org/10.1016/j.jcis.2020.03.123.

[42] J. Cardellini, L. Caselli, E. Lavagna, S. Salassi, H. Amenitsch, M. Calamai, C. Montis, G. Rossi, D. Berti, Membrane phase drives the assembly of gold nanoparticles on biomimetic lipid bilayers, The Journal of Physical Chemistry C 126 (9) (2022) 4483–4494, https://doi.org/10.1021/acs.jpcc.1c08914.

[43] A. Zendrini, L. Paolini, S. Busatto, A. Radeghieri, M. Romano, M.H.M. Wauben, M.J.C. van Herwijnen, P. Nejsum, A. Borup, A. Ridolfi, C. Montis, P. Bergese, Augmented COlorimetric NANoplasmonic (CONAN) method for grading purity and determine concentration of EV microliter volume solutions, Front. Bioeng. Biotechnol. 7 (2020), https://doi.org/10.3389/fbioe.2019.00452.

[44] L. Caselli, A. Ridolfi, J. Cardellini, L. Sharpnack, L. Paolini, M. Brucale, F. Valle, C. Montis, P. Bergese, D. Berti, A plasmon-based nanoruler to probe the mechanical properties of synthetic and biogenic nanosized lipid vesicles, Nanoscale Horizons 6 (7) (2021) 543–550, https://doi.org/10.1039/D1NH00012H.

[45] J. Turkevich, P.C. Stevenson, J. Hillier, A study of the nucleation and growth processes in the synthesis of colloidal gold, Discuss. Faraday Soc. 11 (1951) 55, https://doi.org/10.1039/df9511100055.

[46] D. Maiolo, L. Paolini, G. Di Noto, A. Zendrini, D. Berti, P. Bergese, D. Ricotta, Colorimetric nanoplasmonic assay to determine purity and titrate extracellular vesicles, Anal. Chem. 87 (8) (2015) 4168–4176, https://doi.org/10.1021/ac504861d.

[47] S. Salassi, L. Caselli, J. Cardellini, E. Lavagna, C. Montis, D. Berti, G. Rossi, A martini coarse grained model of citrate-capped gold nanoparticles interacting with lipid bilayers, J. Chem. Theor. Comput. 17 (10) (2021) 6597–6609, https://doi.org/10.1021/acs.jctc.1c00627.

[48] L. Zhang, S. Granick, How to stabilize phospholipid liposomes (using nanoparticles), Nano Lett. 6 (4) (2006) 694–698, https://doi.org/10.1021/nl052455y.

[49] R. Michel, T. Plostica, L. Abezgauz, D. Danino, M. Gradzielski, Control of the stability and structure of liposomes by means of nanoparticles, Soft Matter 9 (16) (2013) 4167, https://doi.org/10.1039/c3sm27875a.

[50] Y. Yu, S.M. Anthony, L. Zhang, S.C. Bae, S. Granick, Cationic nanoparticles stabilize zwitterionic liposomes better than anionic ones, The Journal of Physical Chemistry C 111 (23) (2007) 8233–8236, https://doi.org/10.1021/jp072680z.

[51] S. Thamphiwatana, V. Fu, J. Zhu, D. Lu, W. Gao, L. Zhang, Nanoparticle-stabilized liposomes for pH-responsive gastric drug delivery, Langmuir 29 (39) (2013) 12228–12233, https://doi.org/10.1021/la402695c.

[52] S.V.G. Menon, C. Manohar, K.S. Rao, A new interpretation of the sticky hard sphere model, J. Chem. Phys. 95 (12) (1991) 9186–9190, https://doi.org/10.1063/1.461199.

[53] R.J. Baxter, Percus–yevick equation for hard spheres with surface adhesion, J. Chem. Phys. 49 (6) (1968) 2770–2774, https://doi.org/10.1063/1.1670482.

[54] B. Bharti, J. Meissner, G.H. Findenegg, Aggregation of silica nanoparticles directed by adsorption of lysozyme, Langmuir 27 (16) (2011) 9823–9833, https://doi.org/10.1021/la201898v.

[55] J. Luo, G. Yuan, C. Zhao, CharlesC. Han, J. Chen, Y. Liu, Gelation of large hard particles with short-range attraction induced by bridging of small soft microgels, Soft Matter 11 (12) (2015) 2494–2503, https://doi.org/10.1039/c4sm02165g.